Hindawi
Geofluids
Volume 2021, Article ID 5552169, 14 pages
https://doi.org/10.1155/2021/5552169

Research Article

Effect of Fluid/Rock Interactions on Physical Character of Tight Sandstone Reservoirs during CO_2 Flooding

Dongfeng Zhao and Dandan Yin

School of Petrochemical Engineering & Environment, Zhejiang Ocean University, Zhoushan 316022, China

Correspondence should be addressed to Dongfeng Zhao; dongfeng117@qq.com

Received 16 January 2021; Revised 1 March 2021; Accepted 25 March 2021; Published 15 April 2021

Academic Editor: Yuanyuan Zha

Structures of pore-throat and permeability alteration caused by precipitation and the dissolution of rock matrix are serious problems during CO_2 flooding into reservoirs for enhanced oil recovery (EOR). Experiments were conducted under pressure boost and reduction conditions, which simulate CO_2-brine scaling in different parts of the reservoir during CO_2 flooding. And experiments on the dissolution and scaling of CO_2-brine-rock were carried out. The results show that the pH of brine with CO_2 under high pressure is small, and no precipitation is formed, so there is no precipitation generated near the gas injection well. Pressure drops sharply near the production well, CO_2 dissolved in the formation fluid escapes in large quantities, pH increases, carbonate precipitates are generated, so inorganic scale is formed near the production well. The increase of permeability of core saturated high scale-forming ions is smaller than that of saturated no scale-forming ions brine after CO_2 flooding. The accumulation and attachment of salt crystals were found in some large pores of the core with scale-forming ions water after CO_2 flooding. The ratio of medium size pores decreased, while that of large and small pores increases, and the pore radius distribution differentiates toward polarization.

1. Introduction

Change in injectivity is a problem in CO_2 injection wells, in enhanced oil recovery and sequestration projects, because of reactions between CO_2, brine, and rock [1]. For tight Sandstone Reservoirs, the pores and throats of formation are tiny (the pore-throat radius is about 2~0.03 μm) and the water saturation is high, and the reservoirs are easily damaged. So protecting the tight reservoirs is an important issue.

During CO_2 huff and puff or CO_2 flooding, crude oil, rock, and brine in the reservoir will contact with CO_2 and undergo physical-chemical reactions [1, 2]. Because CO_2 is dissolved in the brine to form carbonic acid, carbonate brine can dissolve the rock matrix in the reservoir. Carbonate minerals and silicate minerals are the main ones dissolved in the matrix, which results in forming new circulation channels and thus increasing the permeability of the stratum [2–5]. It has also been found that the carbonate ion in the formation water and metal ion (Ca^{2+}, Mg^{2+}) produced precipitation which will be deposited on the surface of the rock. Meanwhile, the generated kaolinite, intermediate products, and clay particles dissolved by carbonate cement migrated to pore and throats, and some smaller pores and throats would be blocked, leading to permeability reduction [6–10]. A carbonated water injection field experiment was conducted in Daqing oilfield, and the oil recovery increased by 10.5%. However, due to the scaling and corrosion of injection wells and pipelines were very serious; the field test was finally terminated [11].

The variation trend of rock properties during CO_2 flooding is related to the distribution of pores and throats, brine composition, and thermodynamic conditions, which depends on time and space. So some research results show that CO_2 flooding improved the reservoir, while some considered this technology damages the reservoir. Ross et al. [12] conducted CO_2 flooding experiments on cores of oolitic limestone, calcite, and dolomite, respectively, and the experimental results showed that CO_2 flooding increased core permeability. Sayegh [13] conducted similar experiments, selecting sandstone cores for CO_2 flooding. Permeability first

Table 1: Composition of the formation water.

Ions	HCO_3^-	Cl^-	Ba^{2+}	Sr^{2+}	Ca^{2+}	Mg^{2+}	K^++Na^+	TDS
C,mg/L	109	57831	112	493	22891	76	10943	92455

increase and then increases. Omole et al. [14] studied the interaction between CO_2 and dolomite, and the results showed that the permeability near the injection well increased while that near the production well decreased. They believed that this was due to the massive dissolution of carbonate minerals around the production well and the new secondary minerals forming near the production well. But most of the previous studies focused on the influence of the interaction between carbonate water and rock on the reservoir [15–21] and, rarely, considered the effect of the reaction between CO_2 and the brine with lots of scale-forming ions in the reservoir. Especially for tight sandstone with formation water containing high concentrations of Ca^{2+} and Mg^{2+}, the pore-throat structures are very complex, so it is necessary to study the interaction between formation water and CO_2.

In this work, taking the rocks and formation water of reservoirs in Changqing oilfield as the research objects, experiments of reaction between brine and CO_2 under pressure boost and reduction condition and CO_2 flooding were carried out to study the precipitation formation of CO_2-formation water in the process of pressure rising and falling. The permeability and porosity of cores before and after CO_2 flooding were tested. The rock mineral composition, micromorphology, composition change, and rock pores and throats radius distribution change were analyzed before and after the CO_2 flooding by EDS analysis, SEM electron microscope analysis, and NMR.

2. Experiments

2.1. Materials. According to the composition of Triassic produced water in Block X of Ordos Basin, the composition of brine was tested and shown in Table 1. The purity of CO_2 used in the experiment is 99.99%. Simulated formation water was prepared, and the scale-forming ions (Ba^{2+}, Sr^{2+}, Ca^{2+}, Mg^{2+}) in the formation water are replaced with K^+ and Na^+; the TDS (Total dissolved solids) is still 92455 mg/L.

Cores: the natural core of Triassic X reservoir in Block X of Ordos Basin is adopted. After the cores were cleaned and dried, they are vacuumed for 48 hours and, then, saturated with clean formation water, and the porosity of the cores is obtained. Then, the permeability of the cores is measured by injecting formation water into the cores. As shown in Table 2, the porosity measured ranged from 9.56% to 13.09%, and the absolute permeability ranged from 0.14 to 0.4×10^{-3} μm^2. Mineral composition of the cores is shown in Table 3.

2.2. Experimental Equipment

2.2.1. Experimental Equipment. The structure of the high temperature and high pressure (HTHP) visual reaction vessel is shown in Figure 1. The internal volume of the reaction vessel is 2000 mL, which can withstand the maximum pressure of 70 MPa. The pressure is controlled by the ISCO pump, and the solution changes can be observed through the sapphire visual window. There is a heating device inside the container; the temperature range is 20~180°C. X-ray photoelectron spectrometer (XPS): Thermo Fisher K-Alpha model; the pH meter (BPH-7200) accuracy was 0.01 ± 0.0005, and the standard buffer solution with pH = 4, 7, 9 was used for calibration before and after the experiment. CO_2 was injected into the vessel with formation water and inserted the pH meter. After preheating the solution to the

Table 2: Basic parameters of the core samples.

Core No.	Length, cm	Pore volume, mL	Porosity, %	K, $\times 10^{-3}$ μm^2
1	6.62	3.77	11.61	0.17
2	7.04	3.52	10.17	0.19
3	6.93	4.45	13.09	0.24
4	7.08	3.67	10.56	0.29
5	6.79	4.02	12.07	0.32
6	6.90	3.50	10.34	0.35
7	6.90	3.25	9.56	0.40
8	7.44	3.75	10.27	0.14
9	6.85	3.41	10.13	0.18
10	6.80	4.22	12.64	0.20

Table 3: Mineral composition of the cores.

Mineral	Composition	W, %
Quartz	SiO_2	18.7
Potassium feldspar	$KAlSi_3O_8$	18.2
Anorthose	$NaAlSi_3O_8$-$CaAl_2Si_2O_8$	30.1
Calcite	$CaCO_3$	0.5
Lomontite	CaAl2SiO12·4H2O	4.4
Clay	—	28.1

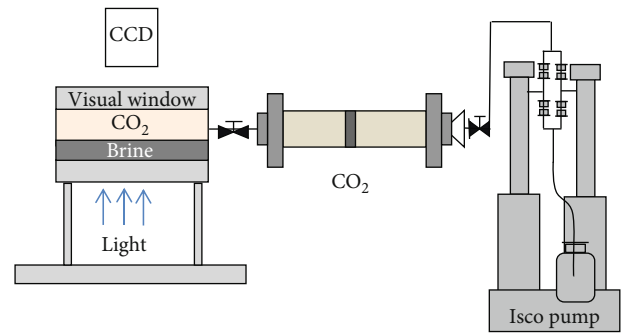

Figure 1: HTHP visual reaction vessel.

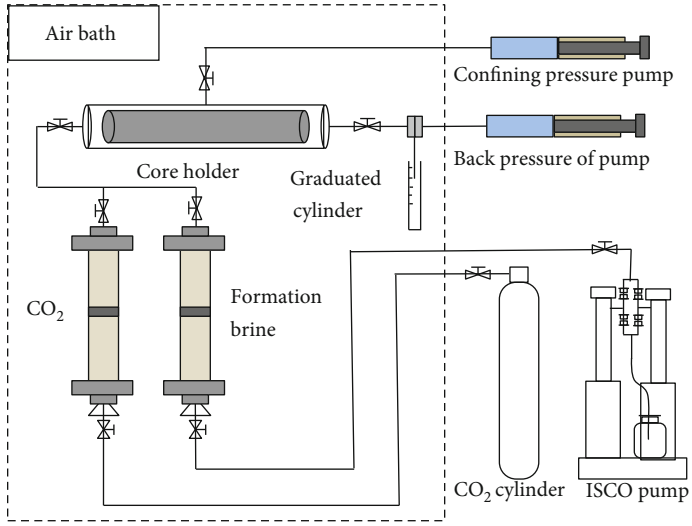

Figure 2: Schematic diagram of the core-flood apparatus.

specified temperature, gradually increase the pressure and record the balance reading displayed on the pH meter at each pressure point.

A schematic diagram of the high-pressure core-flooding apparatus used for CO_2 flooding experiments is shown in Figure 2. Formation water, simulated formation water (water with no scale-forming ions), and CO_2 were contained separately in three high-pressure cylinders. A dual ISCO syringe pump was used to inject fluid from the high-pressure cylinders to the core holder ($P_{max} = 80$ MPa; $T_{max} = 130°C$). A pump was used to maintain confining pressure, and another pump and a back-pressure valve were used together to regulate and maintain the back-pressure. The cylinders and core holder were placed in a constant-temperature oven ($T_{max} = 100.0°C$). The produced brine, oil, and gas were collected and quantified by a gas–liquid cyclone separator and a mass flow meter. Flow data and pressure were logged automatically by a computer during the experiments.

2.3. Experimental Methods and Procedures

2.3.1. Experiments of Reaction between CO_2 and Brine. 250 mL of brine was injected into the HTHP reaction vessel. CO_2 was injected into the reaction vessel through the cylinder. As the pressure changed, precipitation was observed in the solution through the visual equipment. The pH of brine dissolved with CO_2 under different pressures was measured by the pH meter. The precipitate was filtered, dried, pressed, and then measured by X-ray electron spectroscopy (XPS) to determine the elemental composition of the precipitate.

2.3.2. CO_2-Water-Rock Interaction Core Flooding Experiment. The schematic diagram of the core displacement experiment is shown in Figure 3. Before the experiment, the cores were put into the extraction device and cleaned with toluene and methanol to remove oil, salt, and cement. Oil, water, and CO_2 are injected into the cores.

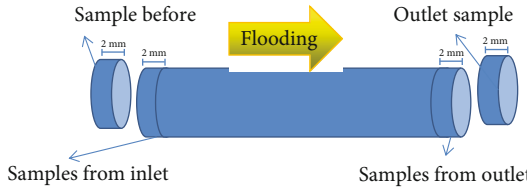

Figure 3: The diagram of core sampling before and after the flooding.

Each group of CO_2 flooding experiment was carried out according to the following steps. First, slices A and D with thickness of 2 mm were cut at the injection end and the outlet end of the core, respectively, as analysis samples. The distribution of pore radius of cores saturated with simulated formation water (water with no scale-forming ions) was determined by NMR. The cores were saturated with formation water and then the permeability was measured. CO_2 and water were injected alternately at experimental temperature and pressure. First, 5 PV (pores volume) CO_2 was injected, and then, 5 PV water was injected. Three cycles of injection were performed. After CO_2 flooding, the cores were cleaned and dried, and pore volume and permeability were tested. And then, the MRI was tested and, then, cut core pieces B and C with a thickness of 2 mm at the injection end and the outlet end of the core, respectively, clean and dry them. Scanning electron micrographs (SEM), surface element, and rock mineral analysis were carried out together with the core sections before the flooding. Replace the core and repeat the above procedure under different conditions. The porosity change rate is defined by Eq. (1). The permeability change rate is defined by the following Eq. (2).

$$\eta_{\varphi} = \frac{\varphi_A - \varphi_{A.0}}{\varphi_{A.0}} * 100\%, \quad (1)$$

where η_{φ} is the porosity change rate, $\varphi_{A.0}$ is before the reaction, and φ_A is the porosity after the reaction.

(a) After 2 days (before CO_2 injection)

(b) After 2 days ($P = 20$ MPa)

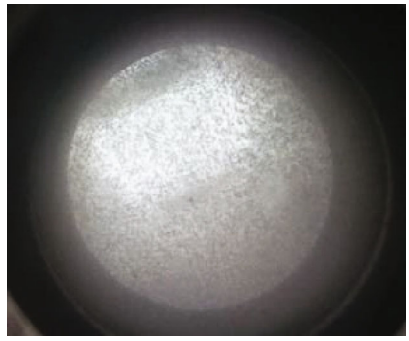

(c) After 2 days (pressure dropped from 20 to 0.1 MPa)

Figure 4: Visual observation of reaction vessel.

$$R = \frac{K_d - K_0}{K_0} * 100\%, \quad (2)$$

where R is the permeability change rate, K_d is the permeability before the reaction, and K_o is the permeability after the reaction.

3. Results and Discussion

3.1. CO_2-Formation Water Interaction. During CO_2 injection, the pressure around the borehole of the gas injection well is high. So a large amount of CO_2 will be dissolved in the formation water in this area. The pressurization can simulate the brine-CO_2 reaction around the injection well. However, the pressure funnel is obvious near the production well, and the sharp pressure drop inevitably causes a large amount of CO_2 dissolved in the formation fluid to escape. To simulate the reaction between formation water and CO_2 when the pressure near the well drops sharply, a pressure-reduced formation water-CO_2 reaction experiment was used. There is an excess of CO_2 throughout the reaction.

To determine whether the brine will precipitate at the formation temperature, pour the formation water into the reaction vessel, keep the temperature at 50°C for 48 h, and then observe through the visual window, no precipitation is observed, as shown in Figure 4(a). CO_2 was injected, increase the CO_2 pressure to 20 MPa, and observe for 12 days, there was no precipitation, as shown in Figure 4(b). Reduce the pressure drops to atmospheric pressure, and precipitation was observed after 2 days, as shown in Figure 4(c). Precipitation is not only deposited on the bottom of the vessel but also a large amount of precipitation is attached to the inner wall of the reaction vessel. CO_2 in the system is in a supercritical fluid state. At the same time, small bubbles containing salt are dispersed in the CO_2 supercritical fluid. When the system is depressurizing, scale precipitates in small water droplets and adheres to the inner wall of the container. Due to the upward flow of CO_2 during pressure relief, the deposition of scale is mainly distributed at the mouth of the container.

The result shows that as the pressure increases, the dissolution of CO_2 in the formation water increases, but there was no precipitation formed. During the depressurization process, precipitation was observed. In response to the above phenomenon, a high-pressure pH test device is used to measure the change in the pH of the CO_2-formation water system during the pressure change under constant temperature conditions. The change in pH with pressure is shown in Figure 5.

The pH of the CO_2-formation water decreases with the increase of pressure as CO_2 is continuously injected. When the pressure is between 0 and 15 MPa, the pH of the solution is between 6.5 and 3.1. This is due to the increase in pressure and the solubility of CO_2 in water, which increases the amount of CO_2 dissolved in water, and more CO_2 reacts with brine to form carbonic acid, thus resulting in the decrease of pH of the solution with the increase of pressure. During the experiment, no precipitation was found in the solution. Although the concentration of Ca^{2+}, Mg^{2+}, and Ba^{2+} divalent ions is relatively high, formation water is acidic because of the injection of CO_2, and CO_2 mainly exists in the form of HCO_3^- and H_2CO_3 (as Eq. (3)–(5)), while the $Ca(HCO_3)_2$ and $Mg(HCO_3)_2$ formed by the combination of HCO_3^- and Ca^{2+} and Mg^{2+} are soluble in water. This indicates that under

the high-pressure near the gas injection well, CO_2 will not react with $CaCl_2$ water-type formation water to produce precipitation. As time goes by, the amount of CO_2 dissolved in the formation water at different positions in the deep part of the reservoir gradually increases, and the pH of the formation water gradually decreases. $CaCl_2$ formation water in the deep part of the reservoir is the same as the near-well area of the gas injection well, and no inorganic precipitation was generated.

$$CO_2(aq) + H_2O \Leftrightarrow H_2CO_3, \quad (3)$$

$$H_2CO_3 \Leftrightarrow H^+ + HCO_3^-, \quad (4)$$

$$CO_2(aq) + OH^- \Leftrightarrow HCO_3. \quad (5)$$

In the near-well zone of the production well, due to the sharp pressure drop, a large amount of CO_2 escapes. When the partial pressure of CO_2 in the solution decreases, the reaction proceeds to the left, and the originally dissolved $Ca(HCO_3)_2$ decomposes to form the $CaCO_3$ scale (as Eq. (6)–(10)). Therefore, during the CO_2 injection, $CaCl_2$ water-type formation water will lead to the formation of inorganic scales near the production well.

$$HCO_3^- \Leftrightarrow H^+ + CO_3^{2-}, \quad (6)$$

$$Ca^{2+} + CO_3^{2-} \Leftrightarrow CaCO_3\downarrow, \quad (7)$$

$$Mg^{2+} + CO_3^{2-} \Leftrightarrow MgCO_3\downarrow, \quad (8)$$

$$Ca^{2+} + Mg^{2+} + 2CO_3^{2-} \Leftrightarrow CaMg(CO_3)_2\downarrow, \quad (9)$$

$$CaCO_3 + H_2O + CO_2(aq) \Leftrightarrow Ca(HCO_3)_2. \quad (10)$$

Some researchers have found that only when the downhole pressure is lower than the bubble point pressure, the $CaCO_3$ scale was found in the produced water of the oilfield [12]. Vetter (1980, 1987) [22, 23] believes that this is because the pressure drops, and CO_2 is flash vaporized from the system, causing the pH value of the system to rise, and the CO_3^{2-} concentration in the system rises accordingly; thus, the system is in a state of supersaturation and begins to precipitate carbonate [8]. Dawe and Zhang [24] believed that as the pressure drops and the gas was released from the liquid, the gas-liquid interface appeared, which promoted the generation of scale. In their experiments, they found that the presence of small bubbles in the experimental system helped the crystallization of $CaCO_3$ and believed that the reason might be that the surface of the small bubbles had a high Gibbs free energy, which can act as a catalyst for the crystallization process [24].

To study the mechanism of CO_2-formation water forming precipitation, starting from checking the Scanning electron microscope (SEM) image of the precipitation, the element and chemical composition of the sediment were analyzed. There are three common crystal phases of calcium carbonate crystals: calcite, vaterite, and aragonite [25]. Some researchers believed that under low-temperature conditions (below 80°C), C_aCO_3 will precipitate out of the water to form the thermodynamically unstable vaterite [26, 27]. It can be seen from the SEM pictures (Figure 5) that the solution produced vaterite crystals which are loose and soft.

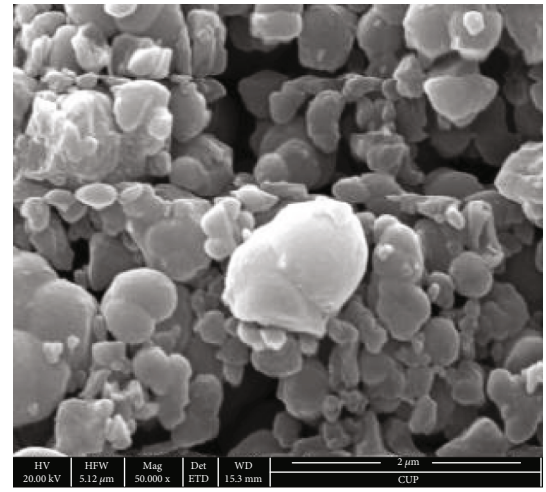

Figure 5: SEM pictures of crystalline phases of precipitation.

Table 4: Content of elements in precipitation.

Element	Ba	Sr	Ca	Mg	C	O
mol %	0.32	2.46	4.74	0.43	47.92	44.13

The precipitate was measured by X-ray electron spectroscopy (XPS), and the measurement results are shown in Table 4. The main elements in the precipitate are C and O, followed by metal elements, mainly Ca, Sr, Mg, and Ba, as shown in Figure 6. According to the ion composition measured by the formation water and the ionization reaction of CO2 dissolving into the formation water to produce CO_3^{2-} and HCO_3^-, it can be concluded that the precipitates mainly consist of $CaCO_3$, $BaCO_3$, $SrCO_3$, $MgCO_3$, $CaMg(CO_3)_2$, etc.

3.2. Effects of CO_2 Flooding on Properties of Rock. Previous scholars conducted high-pressure reaction experiments in cylinders of CO_2-formation water-rock interaction and drew some conclusions about the influence of CO_2-formation water-rock interaction on reservoir physical properties [6, 15, 16]. However, the reactor is a closed system, which cannot reflect the structural characteristics of porous media. Experiments have also been carried out with artificial cores [28–30]. Although there is no water-rock reaction in the artificial tight sandstone core, the pore structure of the artificial low-permeability cores is relatively simple, which cannot simulate the complexity of the pore structure of the tight sandstone cores. Therefore, it is necessary to carry out the formation water-CO_2 flooding experiment in the natural tight sandstone cores. By CO_2 flooding cores saturated with no scale-forming ions water, precipitation generated by brine and CO_2 reaction can be excluded, and the influence of CO_2-water-rock reaction on the physical properties of rock can be obtained. By comparing the cores saturated with no scale-forming ions water and high concentration scale-

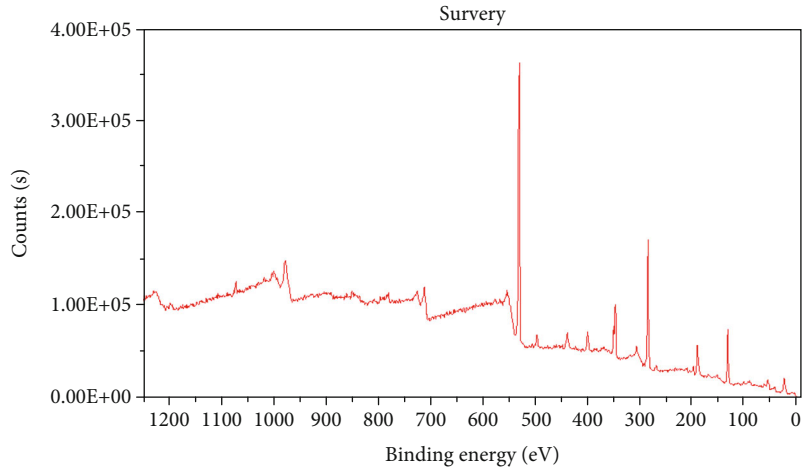

(a) X-ray photoelectron spectroscopy full spectrum

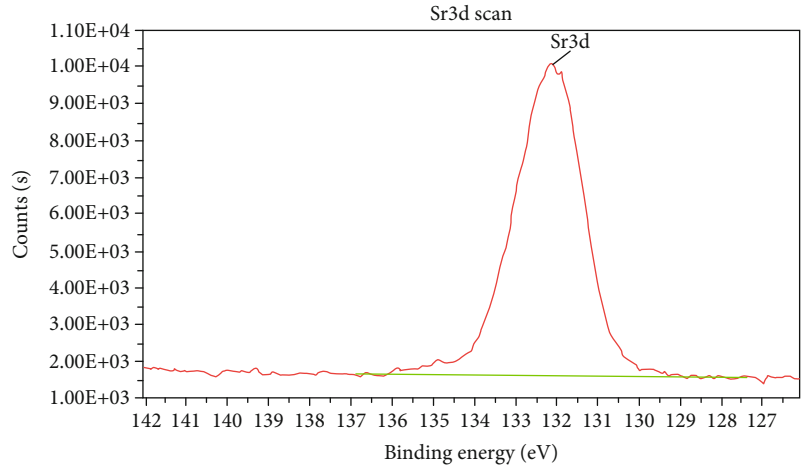

(b) Fine spectrum of element Sr

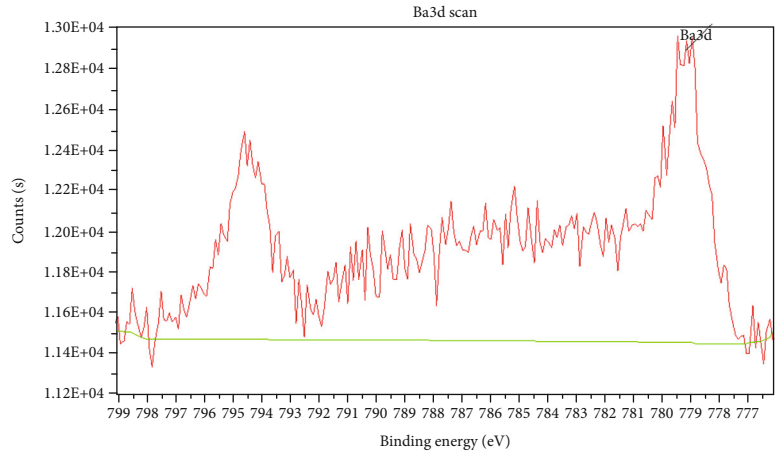

(c) Fine spectrum of element Ba

Figure 6: Continued.

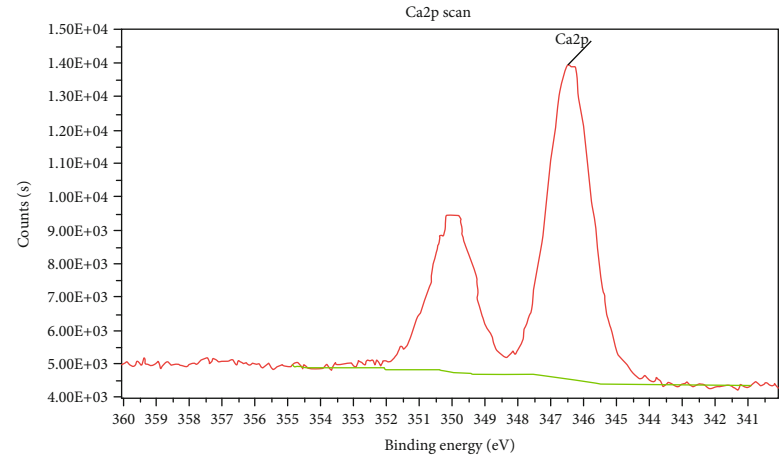

(d) Fine spectrum of element Ca

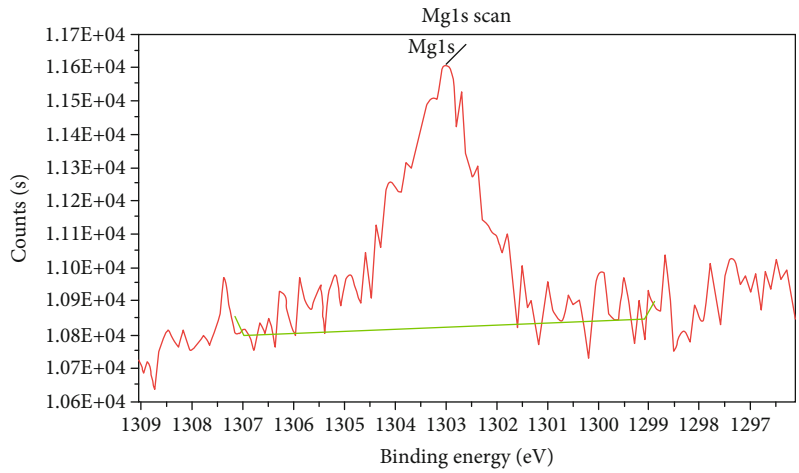

(e) Fine spectrum of element Mg

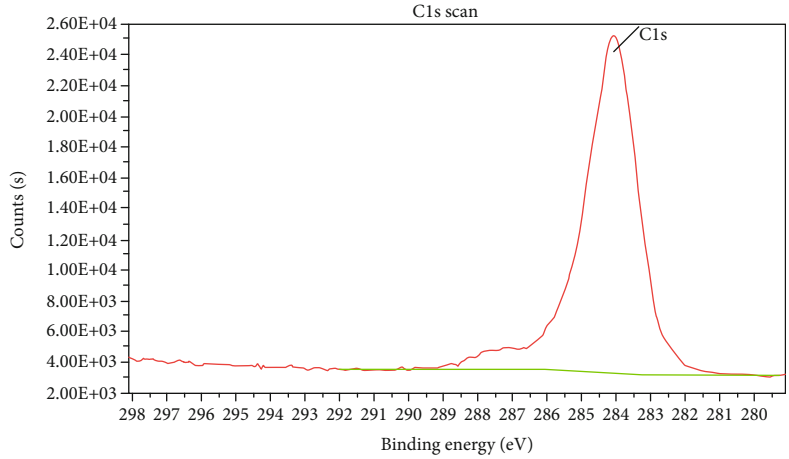

(f) Fine spectrum of element C

Figure 6: Continued.

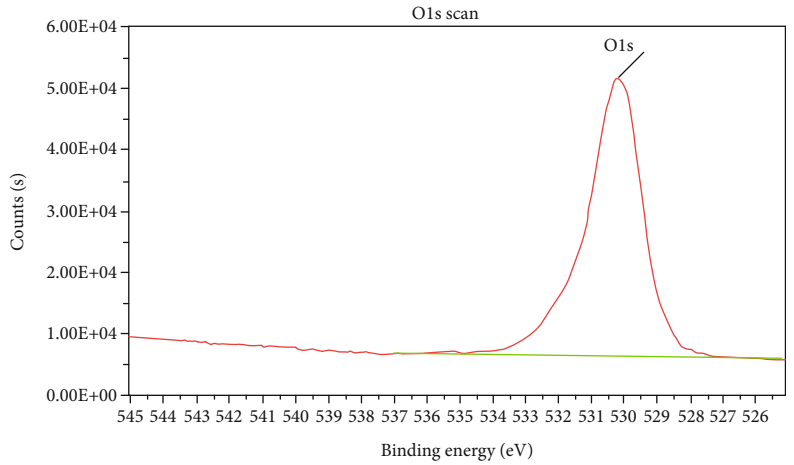

(g) Fine spectrum of element O

Figure 6: X-ray photoelectron spectroscopy spectrum.

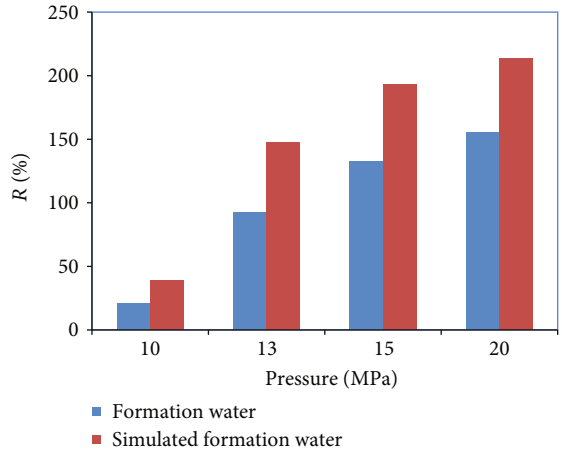

Figure 7: Permeability changing with pressure after CO_2 flooding.

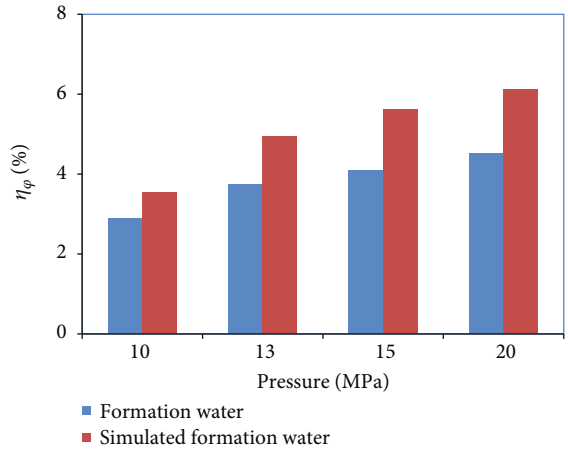

Figure 8: Porosity changing with pressure after CO_2 flooding.

forming ions water flooding experiments, the influence of the precipitation generated by CO_2 and formation water in the reservoir on the physical properties of rock is obtained.

3.2.1. Changes in Core Permeability and Porosity after CO_2 Flooding. The changes in core permeability and porosity after CO_2 flooding were shown in Figures 7 and 8. The permeability and porosity of cores saturated with simulated formation water (no scale-forming ions water) and cores saturated with formation water increased after CO_2 flooding under different pressures. Under the pressure of 15 MPa, the pH of the solution is about 3.1 (as Figure 9), and the permeability of the cores saturated with simulated formation water (no scale-forming ions water) increased by 2 times, and that of the core saturated with formation water increased by 1.5 times, and the higher the flooding pressure was, the more it increased. It can be seen that the effect of mineral dissolution on expanding and connecting pores is greater than the effect of particle migration and sedimentation to plug pores. CO_2 flooding can improve the permeability of the reservoir. And according to Figure 5, the higher the pressure, the greater

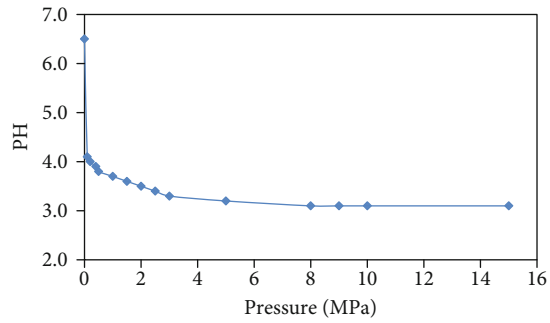

Figure 9: pH of formation water at different pressures during CO2 injection ($T = 50^{\circ}C$).

the solubility of CO_2 in water, the smaller the pH of the solution, and the stronger the CO_2-water-rock interaction. However, the increased permeability of cores saturated with simulated formation water (no scale-forming ions water) is larger than that of the core saturated with formation water, which may be caused by precipitation caused by formation water-CO_2 interaction.

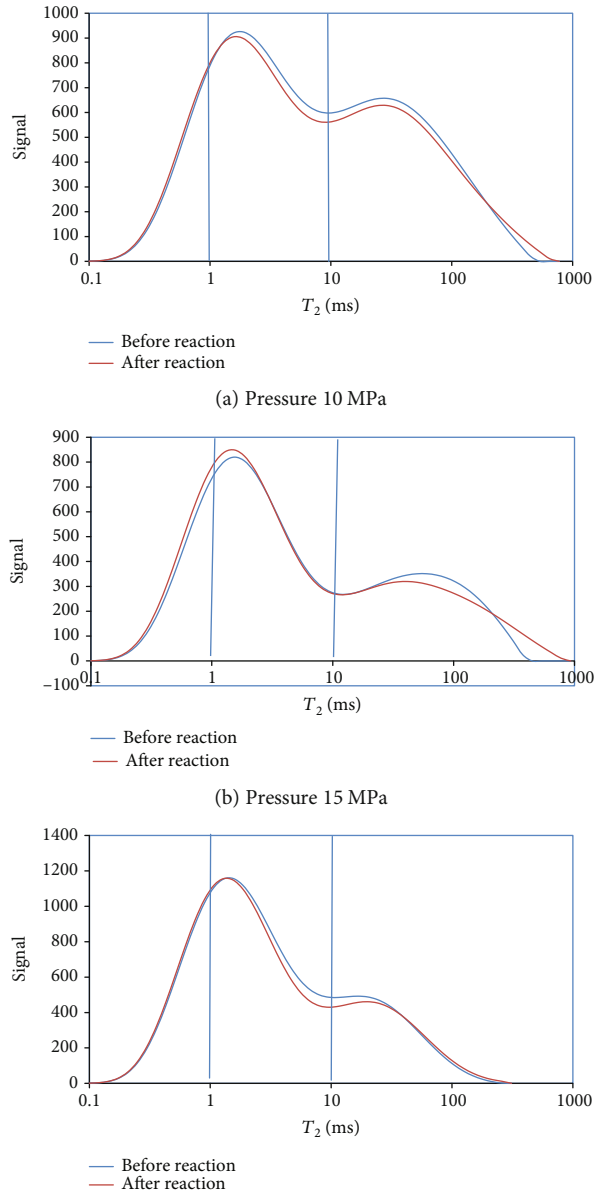

(a) Pressure 10 MPa

(b) Pressure 15 MPa

(c) Pressure 20 MPa

Figure 10: NMRT_2 spectrum of cores saturated with no scale-forming ions water before and after CO_2 flooding.

As shown in Figure 8, the porosity of cores saturated with simulated formation water increased by 6% after CO_2 flooding, with a very small amplitude, while that of core saturated with formation water increased by 2%. These changes are all caused by rock-CO_2-formation water interaction and fluid flooding. Reactions in sandstone rocks generally include dissolution of carbonate minerals, alkaline feldspar, of which mass fraction was 19.7% totally, as shown in Table 3.

$$\begin{aligned} KAlSi_3O_8 + 2H^+ + 9H_2O &= Al_2Si_2O_5(OH)_4 + 2K^+ + 4H_4SiO_4, \\ CO_2 + H_2O + CaCO_3 &\Leftrightarrow Ca(HCO_3)_2, \\ CO_2 + H_2O + MgCO_3 &\Leftrightarrow Mg(HCO_3)_2. \end{aligned} \tag{11}$$

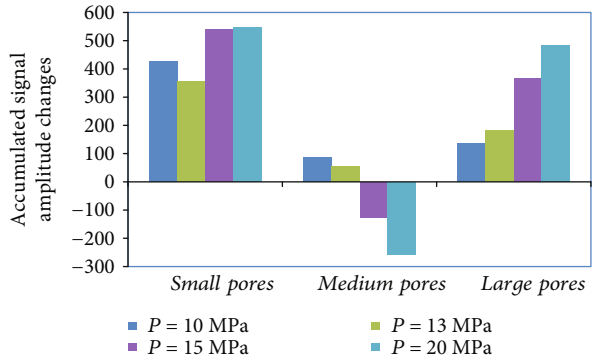

Figure 11: Probability distribution of cores saturated with no scale-forming ions water under different pressures before and after CO_2 flooding.

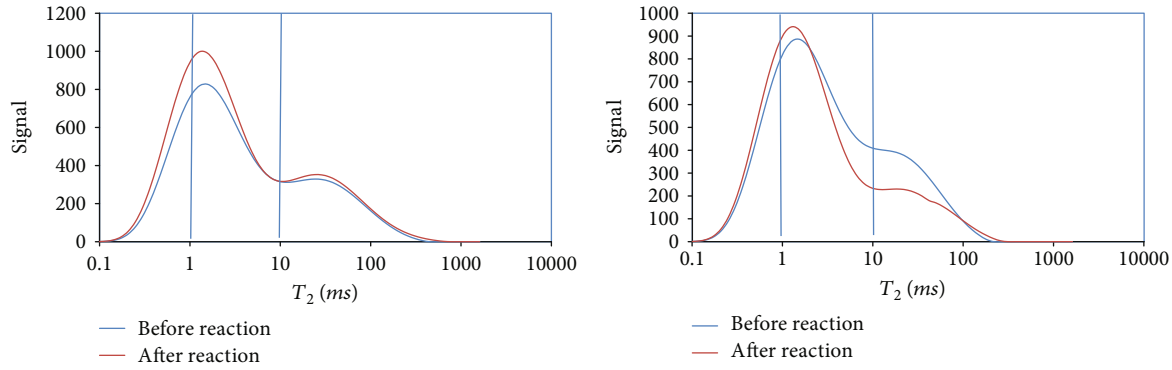

(a) Pressure 10 MPa (b) Pressure 15 MPa

FIGURE 12: NMRT_2 spectrum of cores saturated with formation water before and after CO_2 flooding.

3.2.2. The Changes in Pore-Throat Structure of Cores after CO_2 Flooding. Permeability and porosity are the macroscopic parameters of rock physical properties, and the changes in the overall pore radius distribution of the cores caused by changes in the microscopic morphological structure of pores are the essential factors for changes in rock permeability. To study the effect of interaction between CO_2 and formation water on pore structure, NMR measurements of cores before and after flooding were carried out.

The NMR mechanism shows that the relaxation time (T_2) is proportional to the pore radius (r). Therefore, relaxation time is converted to the pore radius according to Eq. (12) [31].

$$r = \frac{0.735T_2}{C}, \tag{12}$$

where r is the pore radius, m; T_2 is NMR relaxation time, ms; and C is the conversion factor, whose value is 20.23 ms/m. The pore radius distribution curve of T_2 spectrum transformation was well fitted with the conventional mercury injection curve, and the correlation was high.

NMR transverse relaxation time of pores is less than 1 ms defined as small pores. 1-10 ms corresponds to medium pores, and greater than 10 ms corresponds to large pores. The corresponding pore-throat radius is classified as less than 0.36 μm, 0.36~1.82 μm, and greater than 1.82 μm. Figures 10–12 show the NMR spectra of cores saturated with formation water under different pressures before and after CO_2 flooding. It was found that the pore proportion between 0.1-1 ms and 10-1000 ms increased, and the pores proportion between 1 and 10 ms decreased, that is, the probability of large and small pores distribution increased, and the probability of medium pores distribution decreased. For tight reservoirs, on the one hand, macropores are the main flow channels, and the permeability is also determined by the proportion of macropores. The injected CO_2 mainly enters into macro-pores, where the flow rate of CO_2 is relatively high, making it easier for CO_2 to be replenished and updated in time, leading to mineral dissolution, particle release, and pore space enlargement. Meanwhile, there may also be particle migration and pore blockage (the pore space decreases), but

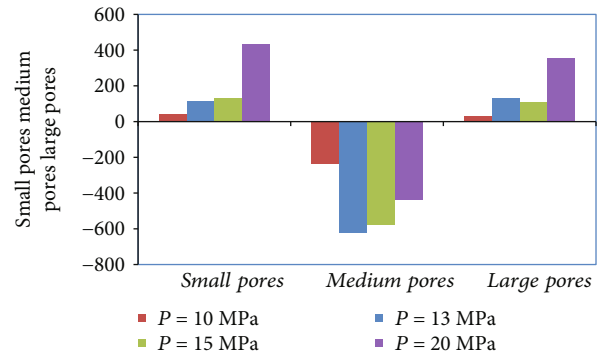

FIGURE 13: Probability distribution of cores saturated with formation water under different pressures before and after CO_2 flooding.

generally, the precipitation is vaterite whose particles soft scale and loose, as shown in Figure 5 which are not enough to block the macropores and have a small probability of blocking the macropores. For medium pores, the reaction degree is bounded between large and small pores. Due to the different connection structures of the medium size pore-throat, the medium size pore-throat eventually differentiates into both ends of large pores and small pores. If the middle pores are connected with more throat channels with a smaller radius, the dissolved small particles in the reaction cannot be migrated well, which will plug up the pores and turn the middle pores into small pores. If the middle pores and macropores are connected, the small particles dissolved because of the reaction can be well transported out, and the middle pores before the reaction will be transformed into macropores. For small pores, on the one hand, CO_2 is a non-wet phase, and the resistance of the Jamin effect should not be ignored when it enters small pores. CO_2 mainly enters small pores through diffusion, and the amount is relatively small, so the change is not obvious. On the other hand, as the minerals in cores react with CO_2, secondary micropores are created. In tight sandstone reservoirs, permeability is mainly contributed by macropores, which are consistent with the previous conclusion that cores permeability increases greatly but porosity changes little after CO_2 flooding.

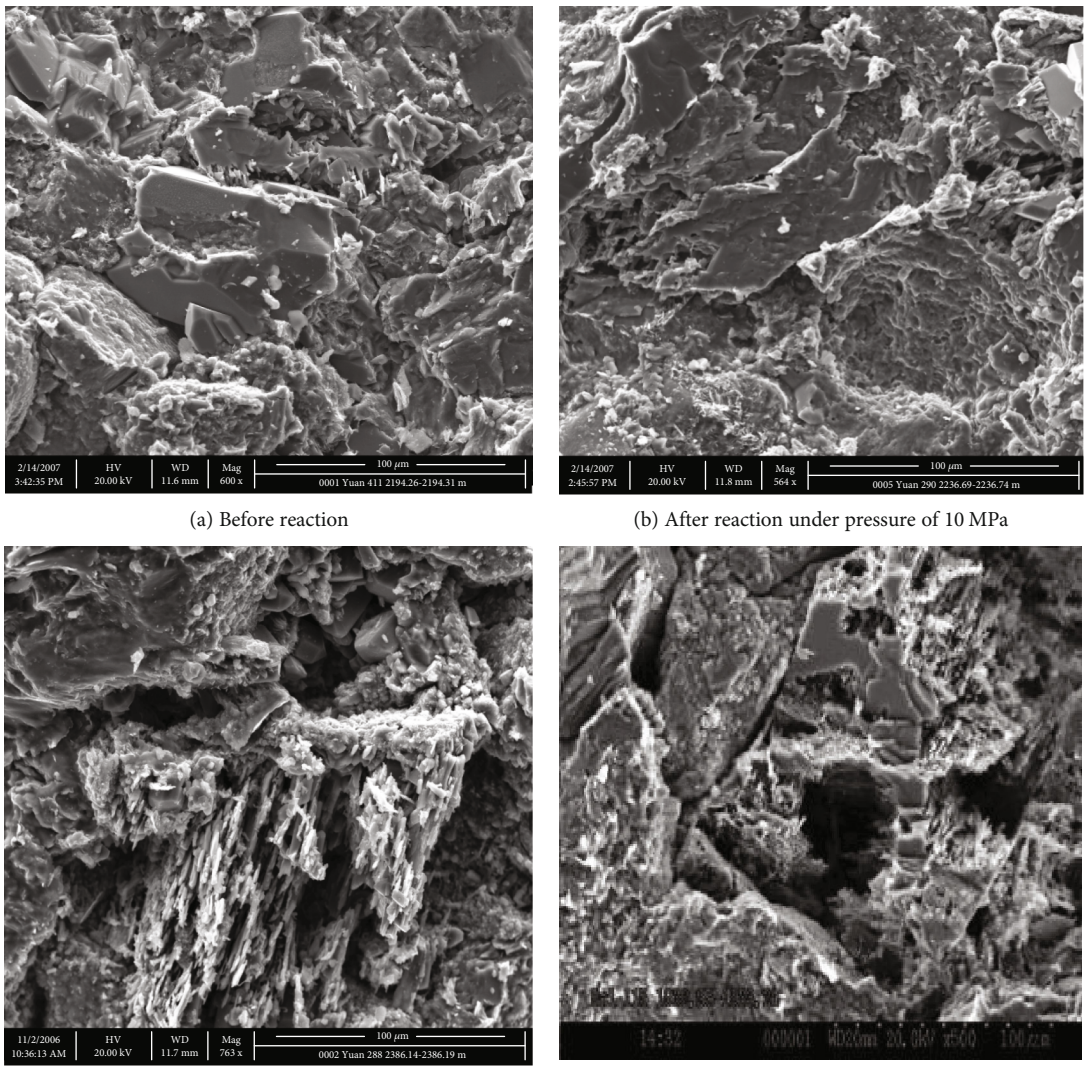

(a) Before reaction

(b) After reaction under pressure of 10 MPa

(c) After reaction under the pressure of 13 MPa

(d) After reaction under the pressure of 15 MPa

Figure 14: SEM pictures of rocks before and after interactions with CO_2, no scale-forming ions water.

Figure 12 shows the variation of the distribution of small, medium, and large pores of cores saturated with formation water before and after CO_2 flooding under different pressures. The proportion of small-medium pores increases, while the proportion of larger medium pores decreases, while the proportion of large medium pores increases, and the proportion of small pores increases. As Figure 12 shown, the probability of small pores distribution increases with the increase of pressure drop, which is caused by the increase of precipitation caused by formation water-CO_2 interaction. The probability amplitude of macropore distribution increases first and then decreases with pressure drop. The decreasing range of porosity distribution probability first increases and then decreases with increasing pressure drop.

Comparing Figure 11 with Figure 13, it can be seen that the reduction of the medium size pore-throat of cores saturated with formation water is larger than that of cores saturated with no scale ionized water after CO_2 flooding, but the increase in the amount of large and small pores is smaller than that after CO_2 flooding with no scale-forming ions water, which is due to metal scaling in the formation water. The reaction between ions and carbonate can form a precipitate in all pores, which results in a decrease in the volume of all types of pores.

3.2.3. Core Surface Morphology Changes after CO_2-Water-Rock Interactions. Figure 14 shows the dissolution of minerals under different flooding pressures because of the interaction of CO_2, water with no scale-forming ions, and rock. As shown in Figure 14(a), before the reaction the crystal shape of the rock is complete and there is a little mineral debris on the quartz surface. After CO_2 flooding, carbonate on the rock surface dissolves, the detrital minerals at the throats in the rock dissolve, the detrital minerals on the rock surface decrease at the back-pressure of 10 MPa, and karst pits appear, as shown in Figure 14(b). With the increase of CO_2 pressure, the dissolution intensifies. After flooding at the back-pressure of 15 MPa, feldspar is more severely dissolved, and the shape of feldspar turns into filamentous, as shown in Figure 14(c). When the flooding pressure increases to

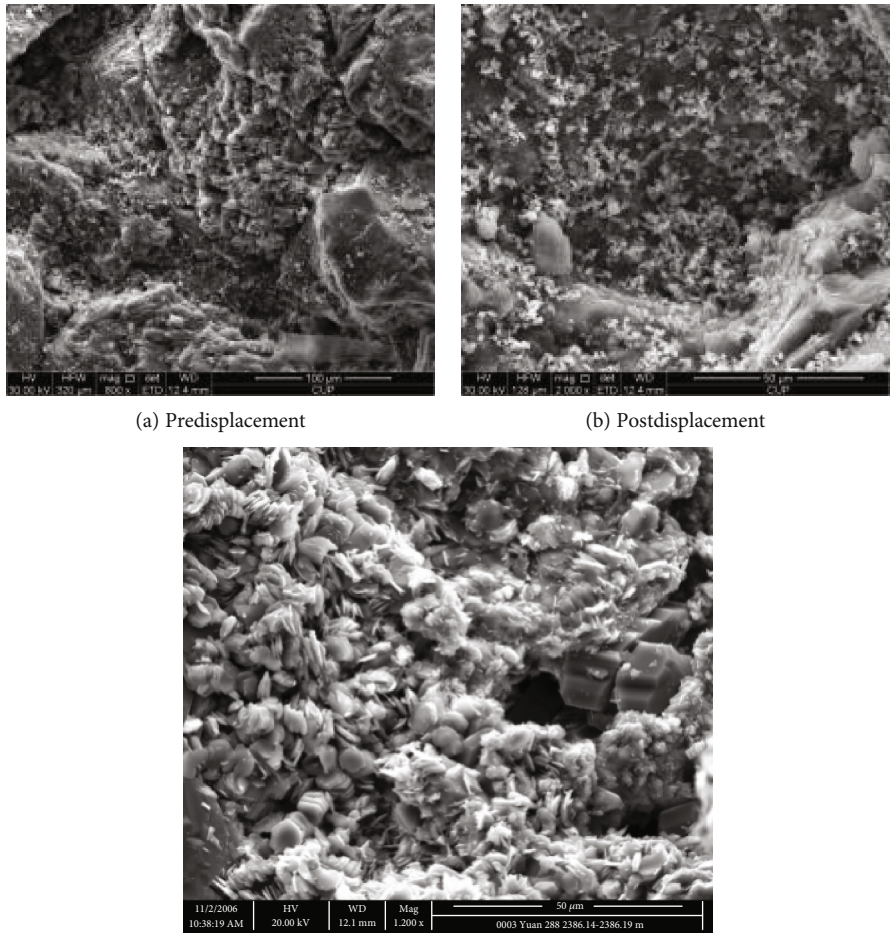

(a) Predisplacement

(b) Postdisplacement

(c) Postdisplacement

Figure 15: SEM pictures of rocks before and after interactions with CO_2, high concentration scale-forming ions water.

20 MPa, carbonate and feldspar are more severely eroded, resulting in some secondary pores in some areas, as shown in Figure 14(d).

The permeability of the reservoir can be improved by increasing the connectivity between pores. The changes of pore morphology caused by the above reasons will seriously affect the permeability of the ultralow-permeability rock, but the porosity will be less affected. In particular, macropore throats, which have a greater contribution to rock permeability, are the main flow channels of fluids and the main sites for particle migration in the process of flooding. Therefore, SEM photographs show that the microstructure of macropores changes significantly, and the distribution of pore radius reflects that proportion of macropores increased.

The rock surface morphology changes after the CO_2-formation-rock interaction (Figure 15(a)–15(c)). SEM showed that some of the precipitates were salt crystal fragments, and these minerals were loosely arranged and did not occupy too much pore space to block the large pore throats (Figures 15(b) and 15(c)). There is good connectivity between the throat and the throat, and this type of pore morphology has little effect on the permeability of the rock. In summary, after CO_2 flooding, the size and morphology of some pores in the core have undergone major changes. The distribution of core pore radius has changed on the entire core scale.

4. Conclusion

The reaction of CO_2 with high mineralization formation water during a pressure-boosting and pressure-reducing were conducted, and the results showed that in the CO_2 injection process, the near-well-bore area of the gas injection well and the deep reservoir because of the pressure rising, the dissolution of CO_2 in the formation water quantity rising, pH of the solution, no precipitate is formed in $CaCl_2$ formation water. However, in the near-well area of the oil well, with the sharp drop of pressure, a large amount of CO_2 dissolved in the formation water will escape, and the pH of the solution will rise, resulting in the formation of inorganic salt precipitation. According to the analysis of X-ray photoelectron spectroscopy, the main components of the precipitation are found to be $CaCO_3$, $BaCO_3$, $SrCO_3$, $MgCO_3$, etc., which is the loose and soft vaterite crystals.

The permeability, porosity, pore throat distribution, and surface morphology changes of the cores saturated formation water and cores of saturated no scale-forming ions water

before and after CO_2 flooding were compared. The results showed that, in Changqing oilfield, the porosity, permeability of cores saturated no scale-forming water, and formation water increased after CO_2 flooding, according to the SEM found that the effect of mineral dissolution pore expansion. Unicom is greater than the effect of particle migration and precipitation of jam pore, even with relatively high-cost scale ion formation, CO_2 injection can still improve the permeability of the reservoir, but the medium size of pore throat turned into large pores and throats, which will aggravate the heterogeneity of strata. For highly mineralized formation water, carbonate precipitation will generate in the core after CO_2 injection, and the change amplitude of permeability, porosity, and core mass is smaller than that after deionized water displacement, carbonate salt crystals are precipitated in the pores.

Data Availability

The data used to support the findings of this study are available from the corresponding author upon request.

Conflicts of Interest

The authors declare no conflict of interest.

Acknowledgments

The authors would like to express their appreciation for the financial support received from the National Natural Science Foundation of China (52004247, 51604243) and Zhoushan Science and Technology Bureau (2021C21024) and the School of Petrochemical Engineering & Environment of Zhejiang Ocean University for permission to publish this paper.

References

[1] J. Perrin, M. Krause, C. W. Kuo, L. Miljkovic, E. Charoba, and S. M. Benson, "Core-scale experimental study of relative permeability properties of CO_2 and brine in reservoir rocks," *Energy Procedia*, vol. 1, no. 1, pp. 3515–3522, 2009.

[2] Y. Zhang, T. Kogure, S. Chiyonobu, X. Lei, and Z. Xue, "Influence of heterogeneity on relative permeability for CO2/brine: CT observations and numerical modeling," *Energy Procedia*, vol. 37, pp. 4647–4654, 2013.

[3] I. Gaus, "Role and impact of CO2–rock interactions during CO2 storage in sedimentary rocks," *International Journal of Greenhouse Gas Control*, vol. 4, no. 1, pp. 73–89, 2010.

[4] M. M. Alam, M. L. Hjuler, H. F. Christensen, and I. L. Fabricius, "Petrophysical and rock-mechanics effects of CO2 injection for enhanced oil recovery: experimental study on chalk from South Arne field, North Sea," *Journal of Petroleum Science and Engineering*, vol. 122, pp. 468–487, 2014.

[5] H. Lin, T. Fujii, R. Takisawa, T. Takahashi, and T. Hashida, "Experimental evaluation of interactions in supercritical CO 2/water/rock minerals system under geologic CO 2 sequestration conditions," *Journal of Materials Science*, vol. 43, no. 7, pp. 2307–2315, 2008.

[6] Z. C. Yu, S. Y. Yang, L. Liu, S. Li, and Y. Z. Yang, "An experimental study on water-rock interaction during water flooding in formations saturated with CO2," *Acta Petrolei Sinica*, vol. 33, no. 6, pp. 1032–1042, 2012.

[7] R. Shiraki and T. L. Dunn, "Experimental study on water-rock interactions during CO_2 flooding in the Tensleep Formation, Wyoming, USA," *Applied Geochemistry*, vol. 15, no. 3, pp. 265–279, 2000.

[8] O. J. Vetter and W. A. Farone, *Calcium carbonate scale in oilfield operations*, Society of Petroleum Engineers, 1987.

[9] O. Izgec, B. Demiral, H. Bertin, and S. Akin, "CO 2 injection into saline carbonate aquifer formations I," *Transport in Porous Media*, vol. 72, no. 1, pp. 1–24, 2008.

[10] O. Izgec, B. Demiral, H. Bertin, and S. Akin, "CO 2 injection into saline carbonate aquifer formations II: comparison of numerical simulations to experiments," *Transport in Porous Media*, vol. 73, no. 1, pp. 57–74, 2008.

[11] Y. Wu, J. J. Carroll, and Z. Du, *Carbon Dioxide Sequestration and Related Technologies*, John Wiley & Sons, 2011.

[12] G. D. Ross, A. C. Todd, and J. A. Tweedie, *The Effect of Simulated CO2 Flooding on the Permeability of Reservoir Rocks*, Enhanced oil recovery. Elsevier, Amsterdam, 1981.

[13] S. G. Sayegh, M. Girard, C. DeBree, and C. DeBree, "Rock/fluid interactions of carbonated brines in a sandstone reservoir: Pembina Cardium, Alberta, Canada," *SPE Formation Evaluation*, vol. 5, no. 4, pp. 399–405, 1990.

[14] O. Oomole and J. S. Osoba, *Carbon Dioxide-Dolomite Rock Interaction during CO Flooding Process*, Petroleum Society of Canada, 1983.

[15] L. Luquot, M. Andreani, P. Gouze, and P. Camps, "CO2 percolation experiment through chlorite/zeolite-rich sandstone (Pretty Hill Formation–Otway Basin–Australia)," *Chemical Geology*, vol. 294, pp. 75–88, 2012.

[16] J. Lu, J. J. Thordsen, J. Horita et al., "CO_2-rock-brine interactions in Lower Tuscaloosa Formation at Cranfield CO_2 sequestration site, Mississippi, U.S.A.," *Chemical Geology*, vol. 291, pp. 269–277, 2012.

[17] L. C. Nielsen, I. C. Bourg, and G. Sposito, "Predicting CO2–water interfacial tension under pressure and temperature conditions of geologic CO2 storage," *Geochimica et Cosmochimica Acta*, vol. 81, pp. 28–38, 2012.

[18] P. Chiquet, J. L. Daridon, D. Broseta, and S. Thibeau, "CO2/water interfacial tensions under pressure and temperature conditions of CO2 geological storage," *Energy Conversion and Management*, vol. 48, no. 3, pp. 736–744, 2007.

[19] Z. Yu, L. Liu, S. Yang, S. Li, and Y. Yang, "An experimental study of CO2–brine–rock interaction at in situ pressure–temperature reservoir conditions," *Chemical Geology*, vol. 326, pp. 88–101, 2012.

[20] P. Mandalaparty, "Reaction Chemistry in Carbon Dioxide Sequestration," *Dissertation abstracts international*, vol. 73, no. 11, p. 13, 2012.

[21] S. Fischer, A. Liebscher, and M. Wandrey, "CO2–brine–rock interaction—first results of long-term exposure experiments at in situ P–T conditions of the Ketzin CO2 reservoir," *Geochemistry*, vol. 70, pp. 155–164, 2010.

[22] O. J. Vetter and V. Kandarpa, *Prediction of CaCO3 Scale under Downhole Conditions*, Society of Petroleum Engineers, 1980.

[23] O. J. Vetter and W. A. Farone, *Calcium Carbonate Scale in Oilfield Operations*, Society of Petroleum Engineers, 1987.

[24] R. A. Dawe and Y. Zhang, "Kinetics of calcium carbonate scaling using observations from glass micromodels," *Journal of*

Petroleum Science and Engineering, vol. 18, no. 3-4, pp. 179–187, 1997.

[25] D. E. Ellis and D. Guenzburger, *The discrete variational method and its application to large molecules and solid-state systems*, Centro Brasileiro de Pesquisas Físicas, 1997.

[26] B. Delley, D. E. Ellis, A. J. Freeman, E. J. Baerends, and D. Post, "Binding energy and electronic structure of small copper particles," *Physical Review B*, vol. 27, no. 4, pp. 2132–2144, 1983.

[27] P. G. Koutsoukos and C. G. Kontoyannis, "Precipitation of calcium carbonate in aqueous solutions," *Journal of the Chemical Society, Faraday Transactions 1: Physical Chemistry in Condensed Phases*, vol. 80, no. 5, pp. 1181–1192, 1984.

[28] J. M. Matter, T. Takahashi, and D. Goldberg, "Experimental evaluation of in situ CO2-water-rock reactions during CO2injection in basaltic rocks: implications for geological CO2sequestration," *Geochemistry, Geophysics, Geosystems*, vol. 8, no. 2, 2007.

[29] S. Vialle, J. Dvorkin, and G. Mavko, "Implications of pore microgeometry heterogeneity for the movement and chemical reactivity of CO 2 in carbonates," *Geophysics*, vol. 78, no. 5, pp. L69–L86, 2013.

[30] Q. Wang, S. Yang, P. W. J. Glover, P. Lorinczi, K. Qian, and L. Wang, "Effect of pore-throat microstructures on formation damage during miscible CO2 flooding of tight sandstone reservoirs," *Energy & Fuels*, vol. 34, no. 4, pp. 4338–4352, 2020.

[31] T. Fang, L. Zhang, N. Liu et al., "Quantitative characterization of pore structure of the Carboniferous–Permian tight sandstone gas reservoirs in eastern Linqing depression by using NMR technique," *Petroleum Research*, vol. 3, no. 2, pp. 110–123, 2018.